



Original Research Article

Accuracy of Turbulent Closure Models in Calculation of Thrust of a Low Reynolds Number Airfoil Used as a Propeller

Adek Tasri

Mechanical Engineering Department, Universitas Andalas, Padang 25163, Indonesia

ARTICLE INFO

Article History:

Received: 06 Februari 2022

Revised: 17 Maret 2022

Available online: 30 April 2022

KEYWORDS

Low Reynolds number

Airfoil

Propeller

CORRESPONDING AUTHOR

E-mail: adek.tasri@eng.unand.ac.id

A B S T R A C T

Unlike in the case of a high Reynolds number airfoil, selecting a turbulent closure model for a low Reynolds number airfoil is still a challenge. A turbulent model used for high Reynolds number airfoil is not necessarily suitable for low Reynolds number airfoil due to the presence of separation bubbles in the low Reynolds number airfoil. In this study, we used two simple turbulent models, Spalart-Allmaras and $k-\omega$, in calculating the thrust coefficient of low Reynolds number airfoil used as a propeller to determine their accuracy. It was found that there was a significant discrepancy between the numerical calculation results by both the turbulent model and the experimental data. The $k-\omega$ was a little more accurate than Spalart-Allmaras turbulent closure model.

1. INTRODUCTION

Unmanned Aerial Vehicles (UAV) have gained popularity in the past decade due to their flexibility and low cost of operation. Studies on AUV components such as the low Reynolds number airfoil are starting to attract the attention of researchers. However, research on low Reynolds number airfoils used in the UAV, especially in the field of numerical solutions, is still lagging compared to high Reynolds number airfoils. The numerical solution method for high Reynolds number airfoil cannot be applied directly to low Re airfoil because there are several different flow conditions. In the low Reynolds number airfoil, the boundary layer is laminar. However, the flow momentum to overcome the adverse gradient

pressure is limited, so separation occurs. The separated flow is unstable; the transition developed immediately downstream of the separation point could produce a turbulent wake. In several low Reynolds number flows, the turbulent shear stress could reduce the adverse pressure gradient and reattach the flow to create a separation bubble. The separation bubbles cause the numerical solution of a low Reynolds number airfoil to be different from a high Reynolds number airfoil, which does not have a separation bubble. Turbulent closure models commonly used in high Reynolds number airfoils may not necessarily be suitable for low Reynolds number flows.

Although from deriving the turbulent model [1], the characteristics of each turbulent model can be seen,

this is still not sufficient to provide the most suitable choice for the low Reynolds number propeller with the separation bubbles. Therefore, the researchers used a different turbulent model for this case. Choudary et al. [2] used k-kl-w model to predict the formation, growth and reattachment of the separation bubble around NACA 0021. Hong and Dong [3] studied the circulation distribution of the DTMD4119 propeller using ANSYS Fluent using the SST k-w model. Tian et al. [4] studied the performance of a double blade wind turbine; the RNG k-e model was used in this study. Saturday et al. [5] performed a numerical simulation using a turbulent SST model to determine the effect of rotating domain thickness on aerofoil thrust and power.

The differences in the selection of turbulent models for flow around the propeller show that the most suitable turbulent model for low Re propeller is still to find. This study tests the performances of the two turbulent models, Spalart-Allmaras and k-w, for the low Reynolds number propeller solution. The performance was measured by comparing the thrust coefficient determined from the numerical simulation with the experiment data.

2. TURBULENT CLOSURE MODEL

The instantaneous velocity of a fluid particle in turbulent flow is commonly modelled as the average velocity plus velocity fluctuations as expressed in Eq. (1) and Eq. (2).

$$\mathbf{u}(x_i, t) = \bar{\mathbf{u}}(x_i) + \mathbf{u}'(x_i, t) \tag{1}$$

$$\bar{\mathbf{u}}(x_i) = \lim_{T \rightarrow \infty} \frac{1}{T} \int_0^T \mathbf{u}(x_i) dt \tag{2}$$

$\bar{\mathbf{u}}(x)$ and $\mathbf{u}'(x, t)$ are a time average velocity and velocity fluctuations. $(\mathbf{u} = u\mathbf{i} + v\mathbf{j} + w\mathbf{k})$ is a velocity vector with u, v, w are velocity components in X, Y and Z directions. Based on the instantaneous velocity, the mass and momentum conservation equations can be written as in Eq. (3) – Eq. (6).

Mass conservation equations:

$$\frac{\partial u}{\partial t} + \text{div}(u\mathbf{u}) = -\frac{1}{\rho} \frac{\partial p}{\partial x} + \frac{\eta}{\rho} \text{div}(\text{grad}(u)) \tag{3}$$

$$\frac{\partial v}{\partial t} + \text{div}(v\mathbf{u}) = -\frac{1}{\rho} \frac{\partial p}{\partial y} + \frac{\eta}{\rho} \text{div}(\text{grad}(v)) \tag{4}$$

$$\frac{\partial w}{\partial t} + \text{div}(w\mathbf{u}) = -\frac{1}{\rho} \frac{\partial p}{\partial z} + \frac{\eta}{\rho} \text{div}(\text{grad}(w)) \tag{5}$$

Momentum conservation equation:

$$\frac{\partial \rho \bar{u}}{\partial t} + \text{div}(\rho \bar{u} \mathbf{u}) = -\frac{\partial p}{\partial x} + \text{div}(\eta \text{grad } \bar{u}) + \left[-\frac{\partial(\overline{\rho u'^2})}{\partial x} + \frac{\partial(\overline{\rho u'v'})}{\partial y} - \frac{\partial(\overline{u'w'})}{\partial z} \right] + S_x \tag{6}$$

$$\frac{\partial \rho \bar{v}}{\partial t} + \text{div}(\rho \bar{v} \mathbf{v}) = -\frac{\partial p}{\partial y} + \text{div}(\eta \text{grad } \bar{v}) + \left[-\frac{\partial(\overline{\rho u'v'})}{\partial x} + \frac{\partial(\overline{\rho v'^2})}{\partial y} - \frac{\partial(\overline{v'w'})}{\partial z} \right] + S_y \tag{7}$$

$$\frac{\partial \rho \bar{w}}{\partial t} + \text{div}(\rho \bar{w} \mathbf{w}) = -\frac{\partial p}{\partial z} + \text{div}(\eta \text{grad } \bar{w}) + \left[-\frac{\partial(\overline{\rho u'w'})}{\partial x} + \frac{\partial(\overline{\rho v'w'})}{\partial y} - \frac{\partial(\overline{w'^2})}{\partial z} \right] + S_z \tag{8}$$

The Reynolds stress tensor in the third term of the right-hand side of the momentum conservation equation causes the equations not to be closed; more variables than the available equations. Several additional equations are needed to define the Reynolds stress tensor for the conservation equations to be closed. The additional equations are known as the turbulent closure equation. Several turbulent closure models have been published in the literature, two of which are, Spalart-Allmaras and $k-\omega$, discussed in this section.

2.1 Spalart-Allmaras Turbulent Closure Model

The model was developed by Spalart and Allmaras [6]. The Spalart-Allmaras model only involves one transport equation to determine the Reynolds stress in Eq. (6) – Eq. (8).

$$-\overline{\rho u'_i u'_j} = 2\eta_t S_{ij} = \rho \tilde{\nu} f_v \left(\frac{\partial \bar{u}_i}{\partial x_j} + \frac{\partial \bar{u}_j}{\partial x_i} \right) \quad (9)$$

u_i represent velocity in rectangular coordinate. S_{ij} is rate of deformation of fluid element; η_t is Eddy viscosity; f_v is wall dumping function; $\tilde{\nu}$ is kinematic Eddy viscosity parameter. The equation for S_{ij} , η_t , f_v and $\tilde{\nu}$ are presented in Eq. (10) to Eq. (13)

$$S_{ij} = \frac{\partial \bar{u}_i}{\partial x_j} + \frac{\partial \bar{u}_j}{\partial x_i} \quad (10)$$

$$\eta_t = \rho \tilde{\nu} f_v \quad (11)$$

$$\frac{\partial \rho \tilde{\nu}}{\partial t} + \text{div}(\rho \tilde{\nu} \mathbf{u}) = \frac{1}{\sigma_v} \text{div}[(\eta + \rho \tilde{\nu}) \text{grad}(\tilde{\nu})] + \frac{1}{\sigma_v} \text{div} \left[C_{b2} \rho \frac{\partial \tilde{\nu}}{\partial x_k} \frac{\partial \tilde{\nu}}{\partial x_k} \right] + C_{b1} \rho \tilde{\nu} \tilde{\Omega} - C_{w1} \rho \left(\frac{\tilde{\nu}}{\kappa y} \right)^2 f_w \quad (12)$$

$$f_v = \frac{\chi^3}{\chi^3 + C_{v1}^3} ; \chi = \frac{\tilde{\nu}}{\nu} \quad (13)$$

where σ_v , C_{b2} , C_{b1} , C_{w1} and κ are constants.

The Spalart-Allmaras model was developed for aerodynamic and turbo machinery applications with mild separation. The model has economic computation for the boundary layer of external aerodynamics and is robust in modeling flow on aerofoil and flows with adverse pressure gradient [7,8].

2.2 $k-\omega$ Turbulent Closure Model

One of the robust $k-\omega$ models was proposed by Wilcox [1,9,10] who used dissipation per unit kinetic energy to determine the Reynolds stress as provided in Eq. (14).

$$-\overline{\rho u'_i u'_j} = 2\eta_t S_{ij} - \frac{2}{3} \rho k \delta_{ij} \quad (14)$$

Where $(\omega = \varepsilon/k)$ is a dissipation per unit kinetic energy and $(\eta_t = (\rho k)/\omega)$ is an Eddy viscosity. ε and k are turbulent dissipation and kinetic energy. The transport equation for ε and k are as in Eq. (15) and Eq. (16).

$$\frac{\partial \rho k}{\partial t} + \text{div}(\rho k \mathbf{u}) = \text{div} \left[\left(\eta + \frac{\eta_t}{\sigma_k} \right) \text{grad}(k) \right] + \left(2\eta_t S_{ij} \cdot S_{ij} - \frac{2}{3} \rho k \frac{\partial u_i}{\partial x_i} \delta_{ij} \right) - \beta^* \rho k \omega \quad (15)$$

$$\frac{\partial \rho \omega}{\partial t} + \text{div}(\rho \omega \mathbf{u}) = \text{div} \left[\left(\eta + \frac{\eta_t}{\sigma_w} \right) \text{grad}(\omega) \right] + \gamma_1 \left(2\rho S_{ij} \cdot S_{ij} - \frac{2}{3} \rho \omega \frac{\partial u_i}{\partial x_j} \delta_{ij} \right) - \beta_1 \rho \omega^2 \quad (16)$$

where σ_k , σ_w , γ_1 , β_1 and β^* are constants.

The $k-\omega$ is widely used in the solutions of the boundary layer region due to several advantages such as the integration of turbulent properties towards the wall does not require a wall-damping function, the turbulent kinetic energy on the wall can be set to zero, and the dissipation per unit kinetic energy tends to infinity on the wall.

3. NUMERICAL SETUP

Numerical simulations were carried out to determine the accuracy of the Spalart-Allmaras and standard $k-\omega$ turbulent model in calculating the thrust coefficient on the low Reynolds number propeller. The thrush coefficient was calculated on several Reynolds numbers and compared with the experiment data conducted by Deter et al. [11] to see both turbulent models' accuracy.

Reynolds number was defined by rotation speed and chord length at 75% blade station as expressed in Eq. (17)

$$\text{Re} = \frac{\rho c_{75} \sqrt{V^2 + (n\pi 0.7D)^2}}{\eta} \quad (17)$$

where ρ and η are air density and viscosity. V , D and n are air velocity, propeller diameter and rotation speed, respectively.

The thrust coefficient was defined as in Eq. (18)

$$C_T = \frac{T}{\rho n^2 D^4} \quad (18)$$

where T is the thrust.

The propeller used in this study is a two-blade NR 640, similar with the propeller used by Deter et al. [11]. The computation domain was modelled as a cylinder with a diameter of five times the propeller's diameter (D). To obtain inflow uniformity, the propeller was located $3.5 D$ from the inlet domain. The outlet domain was placed $10 D$ from the propeller, as shown in Figure 1.

The steady-state numerical simulation was carried out using Ansys Fluent 2021R1. A multiple reference frame (MRF) is used to model the propeller's rotation where the propeller was placed in a rotating domain, while the surrounding air was defined as a static domain.

A 50000 tetrahedron mesh was laid down in the domain with a small mesh to capture the strong properties gradient used around the propeller. The mesh in the rotating domain is shown in Figure 2.

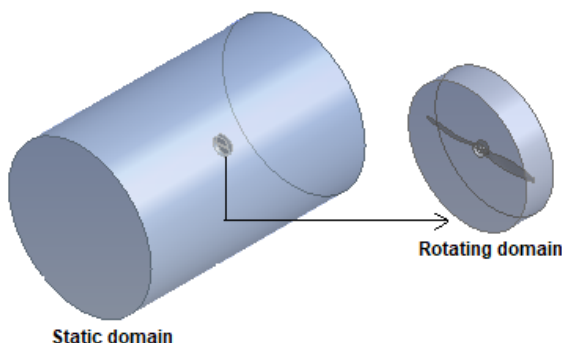


Figure 1. Propeller and calculation domain

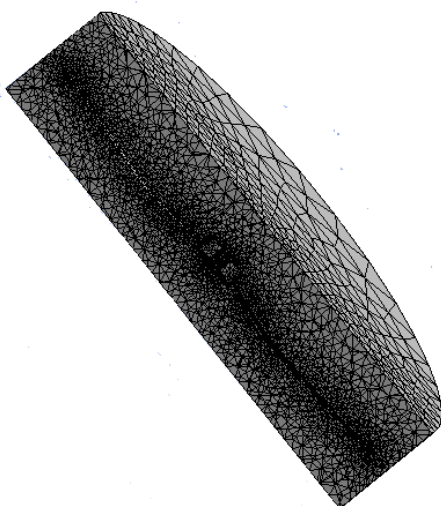


Figure 2. Mesh used in rotating domain

The numerical simulation was carried out in the static condition. Because the velocity at the inlet boundary was unknown for the static condition, the pressure inlet boundary condition was used for the inlet. On the outlet boundary, the pressure outlet condition is specified. A couple algorithm was used to couple continuity and momentum equation and coupling pressure and velocity. Second-order upwind differencing was used in the discretisation of the momentum and pressure correction equation. The first order upwind differencing was used to discretise the turbulent closure equation.

4. RESULT

The numerical simulation results in Figure 3 show that the thrust coefficient obtained using Spalart-Allmaras and $k-\omega$ turbulent model were quite far from the experiment data. The difference between the numerical and experimental results was most likely due to differences in turbulence properties, such as turbulent intensity and length scale, used in numerical calculations with actual values in the experiment. Although the accuracy of both turbulent models was low for the case used in this study, based on the number of the close equation both turbulent models have the advantage of low-cost computation compared to other turbulent models such as the Reynolds stress model.

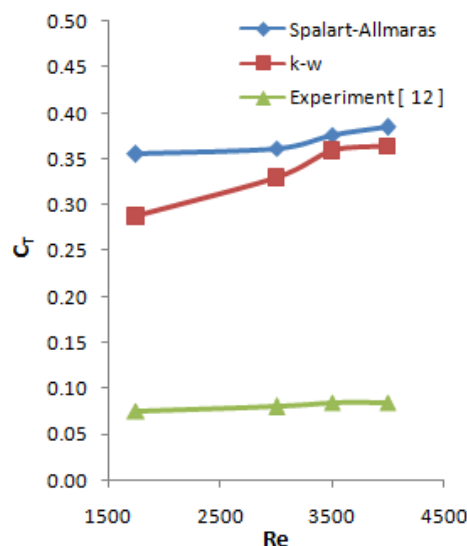


Figure 3. Thrust coefficient of NR 640 propeller

Figure 3 also shows that $k-\omega$ is slightly more accurate than the Spalart-Allmaras model for all range Reynolds numbers used in this study. This condition was presumably caused by the fact that the $k-\omega$ turbulent model is a complete model that provides equations for both k and turbulent length scale; meanwhile, Spalart-Allmaras estimate a turbulent length scale from the typical flow dimension.

5. CONCLUSION

Numerical calculations to determine the thrust coefficient of low Reynolds number airfoil have been carried out using Spalart-Allmaras and $k-\omega$ turbulent model. The following conclusions were drawn:

1. There was a significant discrepancy between the numerical calculation results by both the turbulent model (the Spalart-Allmaras and $k-\omega$) and the experimental data.
2. The $k-\omega$ turbulent model was slightly more accurate than Spalart-Allmaras in calculating the thrust coefficient of low Reynolds number propeller.

REFERENCES

- [1] Wilcox, "Turbulent modeling for CFD," DCW Industries, 1994.
- [2] A. Choudhry, M. Arjomandi, dan R. Kelso, "A study of long separation bubble on thick airfoils and its consequent effects, International Journal of Heat and Fluid Flow, vol. 52, pp. 84–96. 2015, doi: 10.1016/j.ijheatfluidflow.2014.12.001
- [3] F.W. Hong dan S.T. Dong, "Numerical analysis for circulation distribution of propeller blade," Journal of Hydrodynamics, vol. 22, no. 4. pp. 488–493, 2010.
- [4] W. Tian, B. Song, J. VanZwieten, dan P. Pyakurel, "Computational Fluid Dynamics Prediction of a Modified Savonius Wind Turbine with Novel Blade Shapes," Energies, vol. 8, no. 8, pp. 7915–7929, 2015.
- [5] M. Stajuda, M. Karczewski, D. Obidowski dan K. Jozwik, "Development CFD model for propeller simulation," Mechanics and Mechanical Engineering, vol. 20, no. 4 pp.579–593, 2016.
- [6] P. Spalart, dan S. Allmaras, "A one-equation turbulence model for aerodynamic flows". In 30th aerospace sciences meeting and exhibit, 1992.
- [7] P.R. Spalart dan S.R. Allmaras, "A one-equation turbulence model for aerodynamic flows," AIAA, vol. 092, no. 0439, 1992.
- [8] H. K. Versteeg dan W. Malalasekera, "An introduction to computational fluid dynamics: the finite volume method," Pearson Education, 2007.
- [9] D.C. Wilcox, "Reassessment of the Scale-determining Equation for Advanced Turbulence Models," *AIAA J.*, vol. 26, no. 11, pp. 1299–1310, 1998.
- [10] D.C. Wilcox, "Comparison of Two-equation Turbulence Models for Boundary Layers with Pressure Gradients," *AIAA J.*, vol. 31, no. 8, pp. 1414 – 1421, 1993.
- [11] R.W. Deters, G.K. Ananda Krishnan, dan M.S. Selig, "Reynolds number effects on the performance of small-scale propellers," In 32nd AIAA applied aerodynamics conference, 2014.